

# LASER FOCUSING OF ATOMS FOR NANOSTRUCTURE FABRICATION

J. J. McClelland, R. Gupta, Z. J. Jabbour and R. J. Celotta

Electron Physics Group

National Institute of Standards and Technology

Gaithersburg, MD 20899 USA

## ABSTRACT

Laser-focusing of atoms has emerged as a viable form of nanofabrication. Structures are formed by focusing chromium atoms as they deposit onto a surface. The focusing occurs in a standing-wave laser field in one or two dimensions, resulting in arrays spaced at exactly half the laser wavelength ( $\lambda/2 = 212.78$  nm). Atomic force, scanning electron, and transmission electron microscopies are used to view the fabricated structures. Improvements in the technique, including narrowing of the line width and extension to two dimensions are discussed. Theoretical predictions for the shape of the deposited structures are also discussed.

## 1. Introduction

The manipulation of atoms with laser light, part of the burgeoning field of atom optics, has recently been shown to be a useful means of fabricating nanostructures on a surface. Two important features associated with this process have stimulated a great deal of interest: the potential for extremely high resolution, i.e., on the 10 nm scale, and the possibility of massively parallel fabrication, that is the simultaneous fabrication of a large array of high-resolution structures over a large area.

Currently, the methods by which atoms can be focused onto a surface with nanometer-resolution using laser light are the subject of intense investigation. The first suggestion for such a process was made by Balykin and Letokhov (1987), who analyzed the focusing of a sodium atomic beam passing coaxially through the focus of a  $TEM_{01}^*$  (doughnut-mode) laser beam tuned near the atomic resonance. Further analysis of this arrangement (Gallatin and Gould, 1991, McClelland and Scheinfein, 1991) showed that even considering all aberrations, focusing down to a few nanometers should be possible.

The first experimental demonstration of laser-manipulated atomic deposition consisted of crossing a sodium atomic beam with a focused laser beam and observing a "shadow" of the laser beam in the deposited pattern (Prentiss *et al.*, 1992). Shortly afterward, Timp *et al.* (1992) demonstrated that sodium atoms could be focused into a grating-like structure by passing them through a laser standing wave positioned just above a surface. In this configuration each node of the standing wave acts as a "lens" for the atoms, creating an array of lines with spacing of half the laser wavelength (Fig. 1).

In this paper we describe ongoing work on laser focusing of atoms in a standing wave where the atoms being focused are chromium atoms (McClelland *et al.* 1993). The use of chromium atoms has a number of very important advantages for this process, not the least of which are its good adhesion to surfaces, low surface mobility, and stability on exposure to air. These qualities allow direct observation of the deposited nanostructures with a range of diagnostic tools, including atomic force microscopy, and scanning and transmission electron microscopy.

## **2. Light forces on atoms in a standing wave**

The interaction of near-resonant laser fields with atoms results in a rich and varied array of effects on the atomic motion, including laser cooling and trapping, atom interference, quantum optical effects, and of course focusing of atoms (see, e.g., Adams *et al.*, 1994). Exact calculations of atom-field interaction effects can be quite intricate, especially when atoms with multiple levels are involved and lasers with high enough intensity are used to require analysis that includes a significant excited state fraction. Nevertheless, on a basic level the forces can be divided into two general categories: conservative and non-conservative. The conservative force, sometimes referred to as the dipole force, can be thought of classically as arising from the interaction of an induced oscillating electric dipole moment in the atom with a gradient in the oscillating electric field of the laser. The non-conservative forces arise as a result of spontaneous emission, the simplest type being the light pressure force, which comes from repeated absorption of directed momentum from a laser beam and repeated spontaneous emission into random directions.

When the laser is tuned relatively far from the atomic resonance, such that little excited state population is created, the dipole force becomes dominant. In this regime, a two-level atom can be thought of as moving in a conservative potential  $U$ , proportional to the intensity of the laser, given by (Dalibard and Cohen-Tannoudji, 1985)

$$U = \frac{\hbar \Gamma^2 I}{8\Delta I_0}, \quad (1)$$

where  $\Gamma/2\pi$  is the natural line width of the atomic transition (5 MHz for chromium),  $\Delta$  is the detuning of the laser,  $I$  is the laser intensity, and  $I_0$  is the saturation intensity of the atomic transition (83 W/m<sup>2</sup> for chromium).

The conservative potential (1) provides the basis for analyzing the focusing of atoms in a standing-wave from a particle-optics perspective (McClelland 1995). Because the intensity near a node of the standing wave increases quadratically as a function of distance away from the node, the potential to first order provides exactly the right spatial dependence to cause focusing. Fig. 2 demonstrates this by showing exact ray-tracing calculations of chromium atom trajectories through the potential created by a node of the standing wave. It can be seen that, given a perfectly collimated monoenergetic atomic beam and the correct choice of laser power and detuning, an extremely fine focus can be obtained. Of course, the  $\sim 1$  nm width seen in Fig. 2 would be increased by diffraction of the atoms, something that is not taken into account by a particle optics approach. This can be estimated by making an

analogy with the diffraction limit of optical lenses (McClelland *et al.*, 1993); for the conditions of Fig. 2 the diffraction limit is about 10 nm.

### 3. Experiment

Many of the details of the experimental set up and procedure can be found in McClelland *et al.* (1993). Fig. 3 shows a schematic of the apparatus, indicating the major components. A UV-pumped stabilized, single-frequency dye laser with stilbene-420 laser dye generates laser light at 425.55 nm (vacuum wavelength), which matches the  ${}^7S_3 \rightarrow {}^7P_4^o$  transition in atomic chromium (see Fig. 4). The laser light performs two functions. In addition to forming the standing wave, where the laser is tuned 200-500 MHz above the atomic resonance, the laser light is also used to cool the atoms transversely before they enter the standing wave, so that the atomic beam is made as parallel as possible. For this function the laser light is frequency-shifted to about one line width below the atomic transition with an acousto-optic modulator, and polarization gradients (lin  $\perp$  lin) are set up in the cooling region. Collimation angles for the atomic beam as low as 0.14 mrad (full width at half maximum) are obtained in this way, with essentially no loss of flux.

The chromium source is a modified commercial evaporation source. The sample holder and mirror assembly, improved since the original work (McClelland *et al.*, 1993) consists of a single large mirror mounted securely to the sample holder. This mirror serves as the retroreflector for both the laser cooling beam and the standing wave, thereby ensuring alignment between the two. The standing wave laser beam, nominally Gaussian in profile, is

aligned so that it grazes across the sample with its peak intensity at the surface. The deposition substrates consist for the most part of (111) Si wafers either with native oxide or a layer of grown oxide 100 nm thick, although GaAs wafers have also been used.

#### 4. Results and Discussion

After deposition, the samples are removed from vacuum and examined by scanning electron microscopy (SEM) or atomic force microscopy (AFM). Fig. 5 shows two SEM images of the original sample of McClelland *et al.* (1993). These images illustrate the uniformity of the periodicity of the lines (Fig. 5a), and also give some idea of the line shape (Fig 5b).

One major improvement in the deposition process over what was presented in our earlier work has been the reduction of the width of the deposited lines. Using the paraxial particle-optics approximation (McClelland, 1995) it can be shown that the focal length of the lens formed by the standing wave node scales with the  $1/e^2$  radius of the laser beam. By making a tighter laser-beam focus in the deposition region, a shorter atomic-lens focal length is achieved. Just as with light optics, when a shorter focal length lens is used, a smaller focal spot (or line width) results.

Fig. 6 shows an AFM image of the narrower lines obtained by reducing the laser beam waist. For this deposition, the standing wave detuning was +500 MHz, the power was  $33 \pm 3$  mW, and the  $1/e^2$  radius was  $62 \pm 4 \mu\text{m}$  (uncertainty estimates quoted in this paper are to be interpreted as one standard deviation combined random and systematic uncertainties unless

otherwise indicated). The lines in the AFM image of this sample shown in Fig. 6 have an average full-width at half maximum (FWHM) of  $38\pm 1$  nm, compared with the value  $65\pm 6$  nm seen in the previous work. We note that this width does not include any correction for AFM tip shape, so the actual width could be smaller.

Another major advance in the laser-focused atomic deposition process has been the generalization to a two-dimensional array of "dots" (Gupta *et al.*, 1995). Fig. 7 shows an AFM image of these dots, showing the clear periodicity of  $\lambda/2$  (212.78 nm) in two dimensions. The peaks have a height of  $13\pm 1$  nm and a FWHM of  $80\pm 10$  nm. To accomplish this two-dimensional deposition, the standing wave is split into two beams and the second beam is aimed across the sample at  $90^\circ$  relative to the first one. A second mirror mounted on the sample holder retroreflects this beam, forming an additional standing wave in the orthogonal direction.

While the concept of adding another standing wave at  $90^\circ$  to the first one appears relatively simple, some care must be exercised in choice of polarizations for the light fields in order to avoid problems arising from temporal phase instabilities. Since the two standing waves are created by splitting a single laser beam, there will be a definite relative phase relationship between them that depends on the difference in the optical paths taken by the two beams. If this path difference is not stabilized to better than an optical wavelength, vibrations could significantly alter the standing wave pattern. To avoid these problems, we have chosen a polarization configuration where one standing-wave is linearly polarized in the plane of the sample and the other is polarized perpendicular to the sample. In this case, the phase

dependence in the intensity is eliminated, yielding a stable intensity pattern. We note that while the intensity is stable, the local polarization of the field may not be; however the effects of unstable polarization appear to be relatively minor for the current set up.

## 5. Analysis of deposited line shape

In order to further refine and extend the laser-focused atomic deposition process, it is useful to ask how well we can model the line shape of the deposited lines using relatively simple ray-tracing techniques. Line scans of the atomic force microscope images provide a useful source of data for this type of analysis; however, we must be sure that the AFM tip shape is not affecting the profile measurement. To verify the AFM profile, and also to investigate the background level in the depositions, we coated the original sample of McClelland *et al.* (1993) with quartz, sectioned it, and took a transmission electron microscope (TEM) image of it. The result is shown in Fig. 8. Fig. 9 shows a digitization of the line shape from this micrograph (placed on an absolute scale assuming the peak to peak distance is exactly  $\lambda/2$  or 212.78 nm), together with a line scan from an AFM image. The AFM scan was scaled and shifted horizontally and vertically to correct for miscalibrations of the instrument and to account for the background. It can be seen from Fig. 9 that, at least for the line shape of this particular sample, the AFM image gives a quite accurate representation of the true line shape (we note that this may not be true for the narrower lines shown in Fig. 6).

Also shown in Fig. 9 is a deposition profile resulting from a ray-tracing calculation

which attempts to account for the exact experimental conditions. The profile is normalized such that the total area under the curve is equal to the experimental value. Included in the calculation are the measured laser beam detuning, profile and intensity, an assumption of a thermal longitudinal velocity distribution, the measured angular spread of the transversely cooled atom beam, an estimated magnetic sublevel distribution in the Cr atoms (50%  $M=+3$ , 50%  $M=-3$ ), an estimated 16% background of other Cr isotopes, and an estimated 10% background of atoms that decay into the  $^5D_3$  and  $^5D_4$  states during the laser cooling (see Fig. 4). Details of the method of calculation can be found in McClelland (1995).

This calculation attempts to provide a realistic simulation of the actual deposition. As seen in Fig. 9, there is general agreement between the measured and calculated line shapes, and quite good agreement for the background level. Nevertheless, there are some quantitative differences. One source of the deviation between calculation and experiment could be the various simplifications of the theory. The calculations presume an entirely conservative force on the atoms, so any velocity-dependent effects and effects of spontaneous emission are neglected. Also, a semiclassical approach is used, so any effect of the wave-nature of the atoms is ignored. In order to fully explore how important these effects are, it is necessary to perform a fully quantum Monte-Carlo simulation (see, e.g., Marte *et al.*, 1993).

Another potential source of discrepancy is the behavior of the chromium atoms after they strike the surface. It is conceivable that some surface diffusion occurs between the time of deposition and the time of observation, causing the profile to alter its shape. In order to investigate this, we use the equation for one-dimensional surface diffusion (Mullins, 1957)

$$\frac{\partial y}{\partial t} = -BF(y', y'', y''', y''''') + f(x), \quad (2)$$

where  $y$  is the surface height,  $x$  is the distance along the surface, primes denote differentiation with respect to  $x$ ,  $B$  is the surface diffusion coefficient,  $f(x)$  is the flux of atoms striking the surface, and  $F$  is given by

$$F(y', y'', y''', y''''') = \frac{\partial}{\partial x} \left[ (1+y'^2)^{-1/2} \frac{\partial}{\partial x} \left( \frac{y''}{(1+y'^2)^{1/2}} \right) \right]. \quad (3)$$

Letting the surface diffusion constant  $B$  be a free parameter and taking the incident flux  $f(x)$  as predicted by the ray-tracing calculation, we solved eq. (2) numerically, attempting to produce a profile that matched the experimental result. The profile that most closely matched the experiment is shown with a dashed line in Fig. 9. It can be seen that there is a significant qualitative difference between the surface-diffused profile and the data: while the data has a sharp peak at the center, the theoretical curve is far more rounded. From this we can conclude that the measured line profile is not consistent with a surface-diffused profile because the strongest effect of surface diffusion is to round-off sharp features, which the data clearly still exhibits.

With the current analysis, we cannot definitively identify the source of discrepancy between the calculation and experiment, except to say that it is most likely not surface diffusion or AFM tip effects. A likely candidate may be a transverse atomic velocity

distribution with high velocity tails that are not taken into account in the initial conditions of the calculation. Other effects, such as diffraction of the atoms, non-adiabatic effects and velocity-dependent forces cannot be ruled out, however (see, e.g., Marte *et al.*, 1993).

## 6. Future prospects

The results discussed in this paper represent a few of the first experiments in a field with a good potential for rapid expansion. Several future directions appear promising for this type of work, covering areas ranging from fundamental atomic physics to practical fabrication techniques.

From an atomic physics point of view, the deposition of chromium atoms on a surface and the subsequent measurement of the profile on a microscopic scale provides a new, direct method for investigating the localization of atoms in an optical field. Because surface diffusion appears to be relatively insignificant, it is reasonable to interpret the thickness of the chromium on the surface as a measure of the density of atoms in the laser field. This type of measurement can lead to new insights into the behavior of atoms in near-resonant light fields.

From a fabrication point of view, there are a number of directions in which this process can be envisioned as expanding. These fall into two general categories: extension of the techniques to other materials, and the generalization to more complex patterns. Other materials are accessible either by using different atomic beams, such as aluminum (McGowan *et al.*, 1994), or by transferring the chromium patterns to other substrates by using

the chromium as an etch mask. Another interesting possibility is the use of metastable atoms, which can be laser manipulated in similar ways to chromium, to expose a lithographic resist (Berggren *et al.*, 1995). More complex patterns might be created by either improving the dot size in the two-dimensional deposition and scanning the substrate to draw an arbitrary pattern that will be reproduced in each unit cell of the deposition, or by custom-tailoring a light field by combining many laser beams to make the desired pattern by a complicated interference pattern.

Finally, we mention an important application of the Cr lines and/or dots that are currently produced. Because the structures faithfully reproduce the periodicity of the standing wave, which is determined solely by the wavelength of laser light locked to an atomic resonance, the resulting gratings can be used as absolute calibration artifacts on the nanometer scale. While a thorough error analysis is still to be done, casual examination of the deposition process suggests that the accuracy of the pitch of the gratings should be at least a few parts in  $10^5$ , if not better. Such an artifact fills a real need in the microelectronics and storage industry, where high accuracy is essential for densely packing electronic circuits and storage bits.

The authors wish to thank Andrew Zangwill for suggesting the surface diffusion analysis of the deposited line shape. Z. J. J. acknowledges support of a National Research Council postdoctoral fellowship. This work is supported in part by the Technology Administration of the U. S. Department of Commerce, and by the National Science Foundation under grant no. PHY-9312572.

## REFERENCES

Adams CS, Sigel M, and Mlynek J (1994) Phys. Rep. **240**, 143.

Balykin VI and Letokhov VS (1987) Opt. Commun. **64**, 151.

Berggren KK, Bard A, Wilbur, JL, Gillaspay, JD, Helg, AG, McClelland, JJ, Rolston SL, Phillips WD, Prentiss M, and Whitesides, GM (1995) Science, **269**, 1255.

Dalibard J and Cohen-Tannoudji C (1985) J. Opt. Soc. Am. B **2**, 1707.

Gallatin GM and Gould PL (1991) J. Opt. Soc. Am. B **8**, 502.

Gupta R, McClelland JJ, Jabbour ZJ, and Celotta RJ (1995) Appl. Phys. Lett **67**, 1378.

Mullins WW, (1957) J. Appl. Phys. **28**, 333.

Marte P, Dum R, Taïeb R, Lett PD, and Zoller P (1993), Phys. Rev. Lett. **71**, 1335.

McClelland JJ and Scheinfein MR (1991), J. Opt. Soc. Am. B **8**, 1974.

McClelland JJ, Scholten RE, Palm EC, and Celotta RJ (1993) *Science* **262**, 877.

McClelland JJ (1995), *J. Opt. Soc. Am B* **12**, 1761.

McGowan RW and Lee SA (1994), in *Abstracts of Contributed Papers, ICAP XII*, Boulder, CO, July 31-August 5, 1994, p. 2H-7.

Prentiss M, Timp G, Bigelow N, Behringer RE, and Cunningham JE (1992), *Appl. Phys. Lett.* **60**, 1027.

Scholten RE, McClelland JJ, Palm EC, Gavrin A, and Celotta RJ (1994) *J. Vac. Sci. Technol. B* **12**, 1847.

Timp GL, Behrenger RL, Tennant DM, Cunningham JE, Prentiss, M, and Berggren KK (1992) *Phys. Rev. Lett.* **69**, 1636.

## FIGURES

Figure 1. Schematic of laser-focused atomic deposition process.

Figure 2. Trajectory calculation of laser focusing of chromium atoms in a standing wave with a Gaussian envelope. A series of trajectories are shown for varying initial  $x$ -values. All trajectories are given the same initial velocity of 926 m/s and zero initial angle relative to the  $z$ -axis. Also shown is a plot of the atomic flux at the focal plane assuming a uniform flux entering the lens, and laser beam profiles  $I(x,z)$  along  $\hat{x}$  (bottom) and  $\hat{z}$  (left).

Figure 3. Schematic of laser-focused atomic deposition apparatus, showing dye laser, acousto-optic modulator (AOM), miscellaneous optics (including quarter-wave plates, denoted by  $\lambda/4$ ), vacuum chamber, Cr source, deposition substrate and sample holder.

Figure 4. Energy levels of Cr, showing the resonant  ${}^7S_3 \rightarrow {}^7P_4^o$  transition at 425.43 nm (425.55 nm in vacuum).

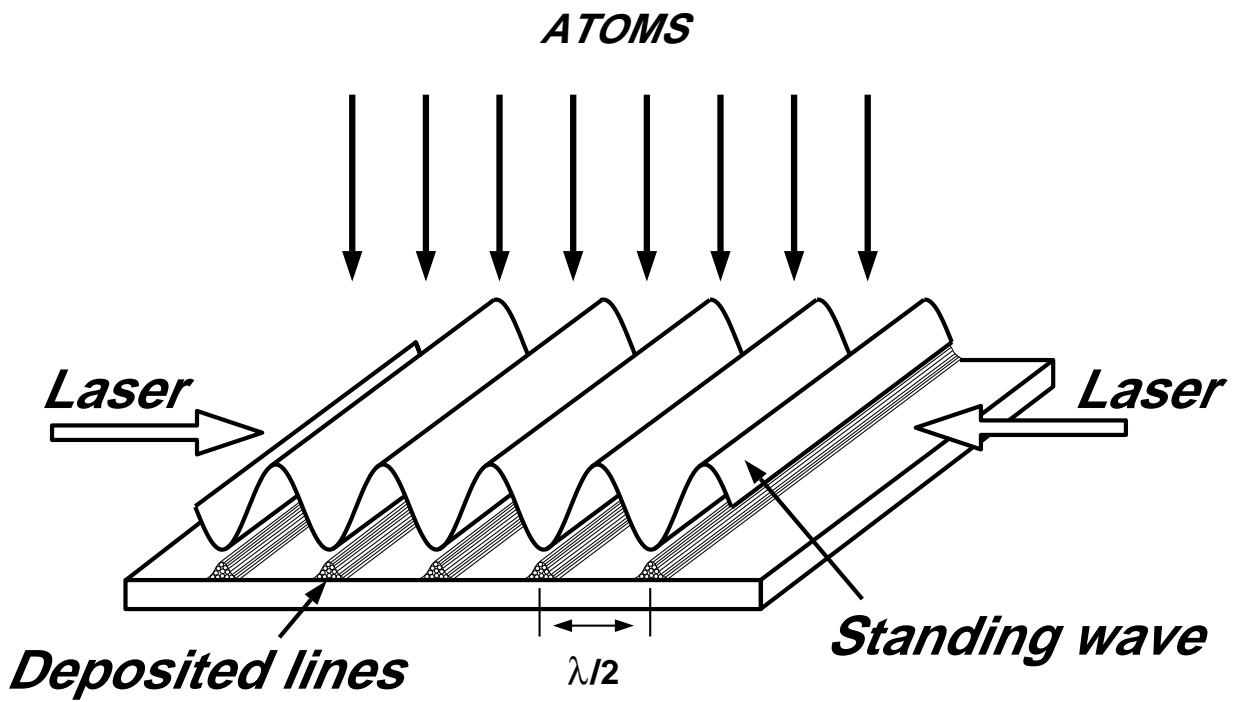
Figure 5. Scanning electron microscope images of Cr structures made by laser-focused atomic deposition. (a) Plan view, illustrating uniformity of lines; (b) close-up of a single line, viewed from an angle.

Figure 6. Atomic force microscope image of Cr lines formed by laser-focused atomic deposition, showing narrowed line width (note this is not the same sample as shown in Fig. 5). The lines in this image have a height of  $8\pm 1$  nm (the vertical scale has been expanded to enhance visibility).

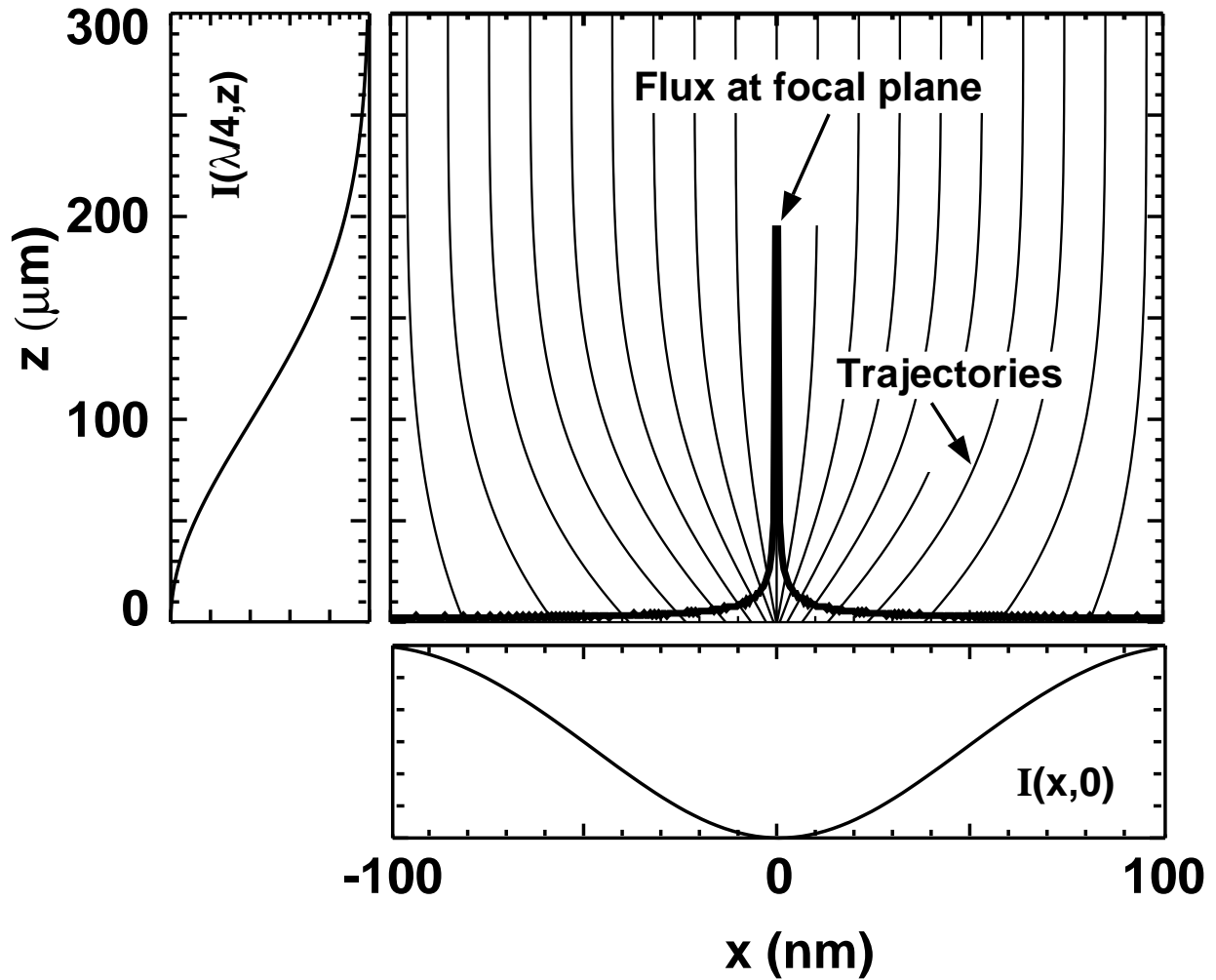
Figure 7. Atomic force microscope image of two-dimensional array formed by laser-focused atomic deposition of Cr. The two perpendicular standing waves are oriented at  $\pm 45^\circ$  relative to the horizontal image axis.

Figure 8. Transmission electron microscope image of Cr lines formed by laser-focused atomic deposition. Shown is a cross section of the sample described in McClelland *et al.* (1993), obtained by coating the sample with quartz and sectioning it.

Figure 9. Line profiles of a single line in laser-focused atomic deposition. The TEM profile is taken directly from Fig. 8. The AFM profile is taken from McClelland *et al.* (1993), scaled and shifted to correct for miscalibrations of the instrument and to account for the background. The calculation is the result of a ray tracing calculation (see text), and the diffusion profile is the result of a diffusion calculation applied to the ray-tracing result (see text).



**Figure 1.** Schematic of laser-focused atomic deposition process.



**Figure 2** Trajectory calculation of laser focusing of chromium atoms in a standing wave with a Gaussian envelope. A series of trajectories are shown for varying initial  $x$ -values. All trajectories are given the same initial velocity of 926 m/s and zero initial angle relative to the  $z$ -axis. Also shown is a plot of the atomic flux at the focal plane assuming a uniform flux entering the lens, and laser beam profiles  $I(x, z)$  along  $\hat{x}$  (bottom) and  $\hat{z}$  (left).

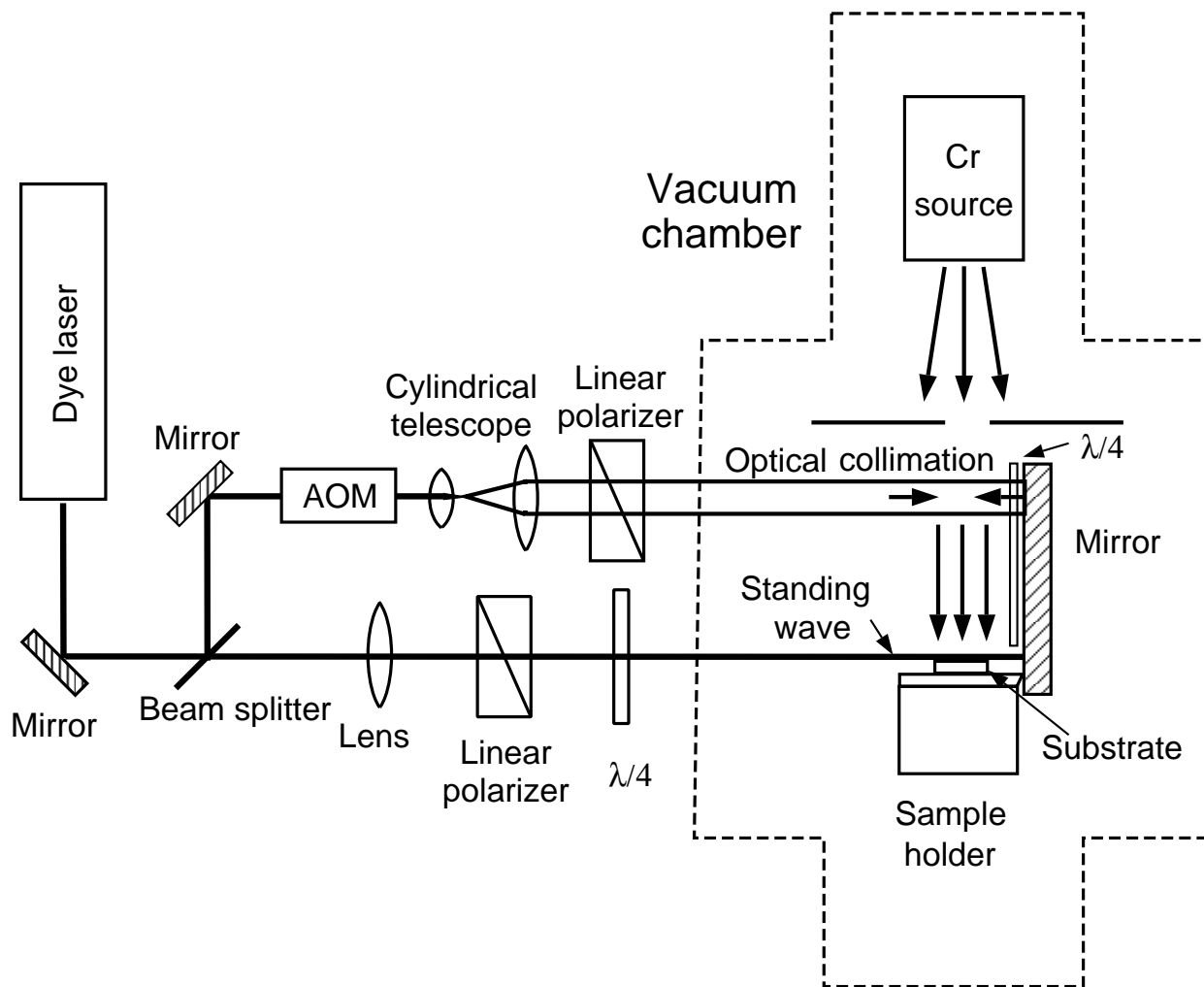


**Figure 3** Schematic of laser-focused atomic deposition apparatus, showing dye laser, acousto-optic modulator (AOM), miscellaneous optics (including quarter-wave plates, denoted by  $\lambda/4$ ), vacuum chamber, Cr source, deposition substrate and sample holder.

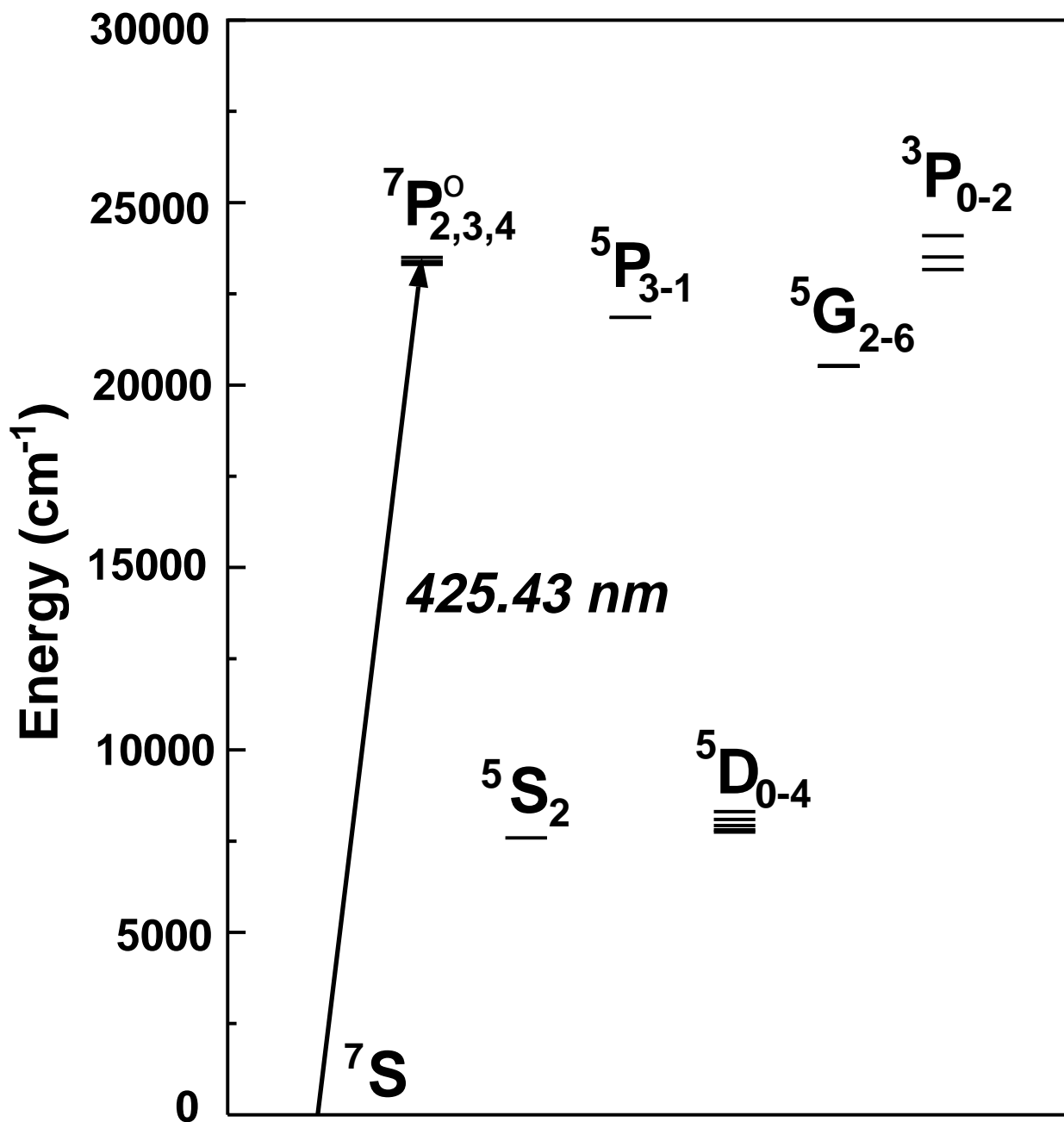


**Figure 4** Energy levels of Cr, showing the resonant  ${}^7\text{S}_3 \rightarrow {}^7\text{P}_4^0$  transition at 425.43 nm (425.55 nm in vacuum).

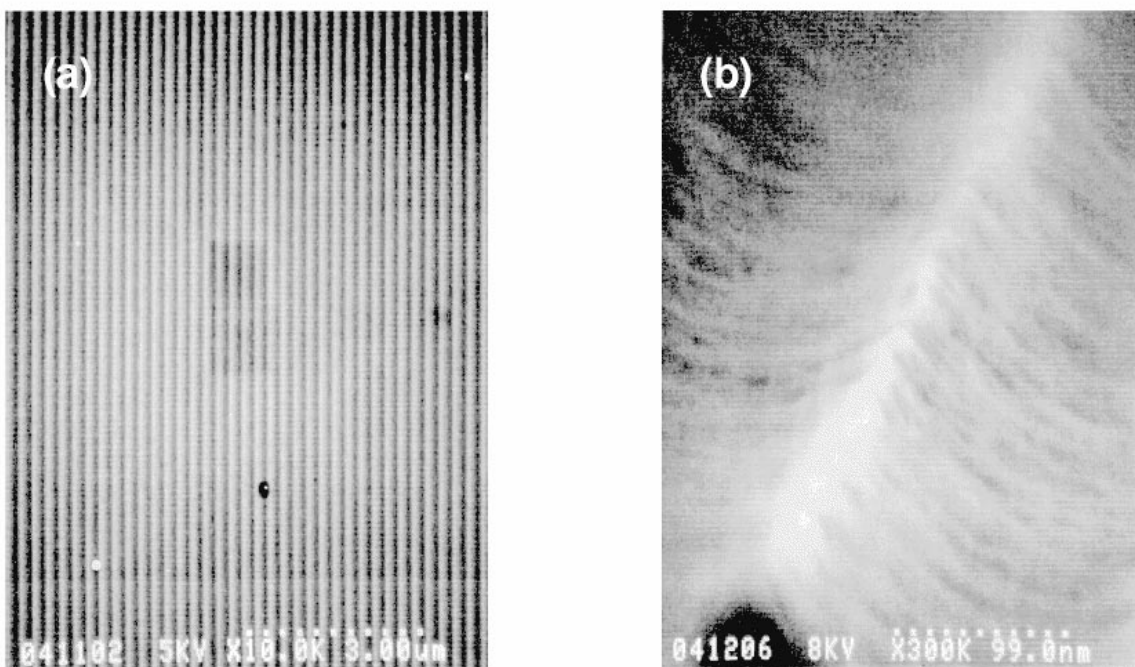


**Figure 5** Scanning electron microscope images of Cr structures made by laser-focused atomic deposition. (a) Plan view, illustrating uniformity of lines; (b) close-up of a single line, viewed from an angle.

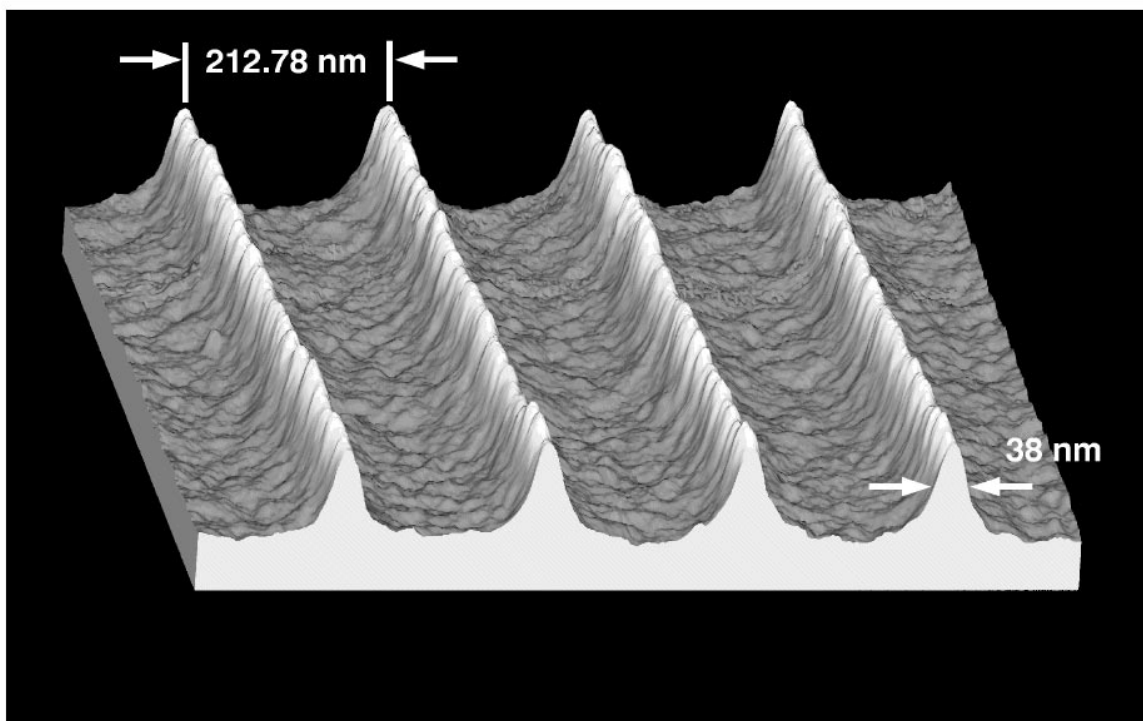


**Figure 6** Atomic force microscope image of Cr lines formed by laser-focused atomic deposition, showing narrowed line width (note this is not the same sample as shown in Fig. 5). The lines in this image have a height of  $8\pm 1$  nm (the vertical scale has been expanded to enhance visibility).

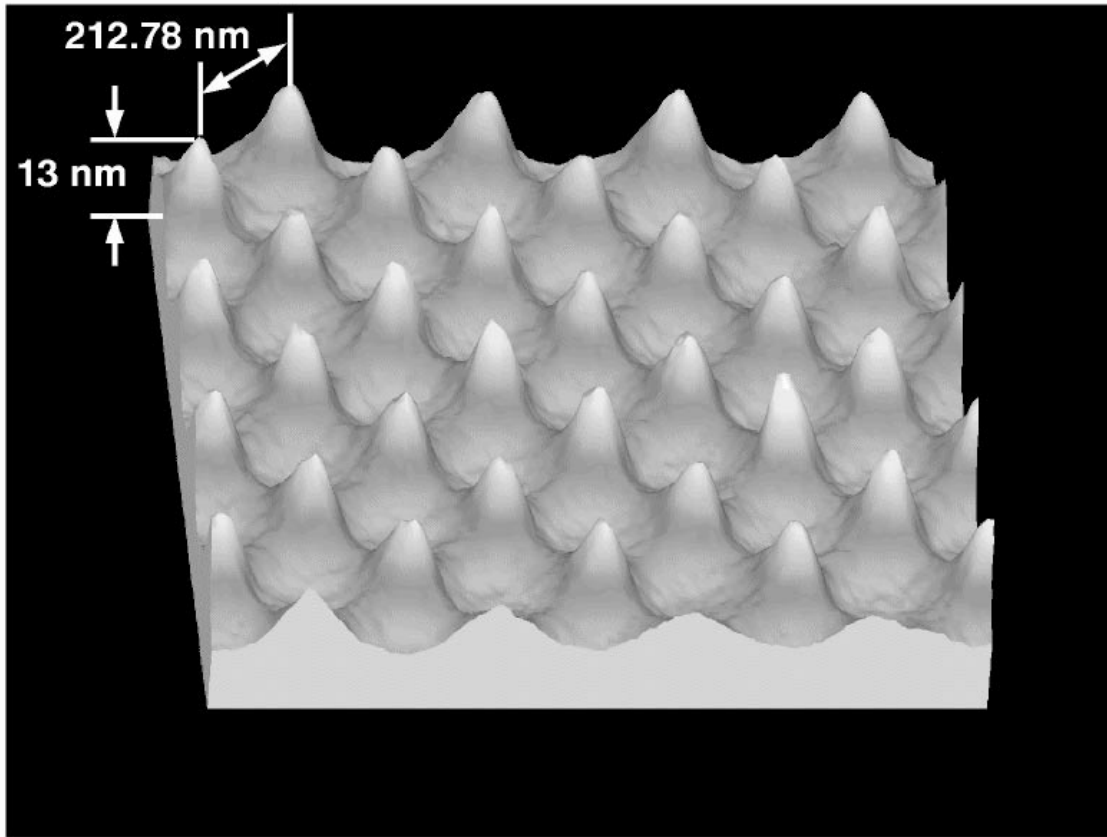


**Figure 7** Atomic force microscope image of two-dimensional array formed by laser-focused atomic deposition of Cr. The two perpendicular standing waves are oriented at  $\pm 45^\circ$  relative to the horizontal image axis.

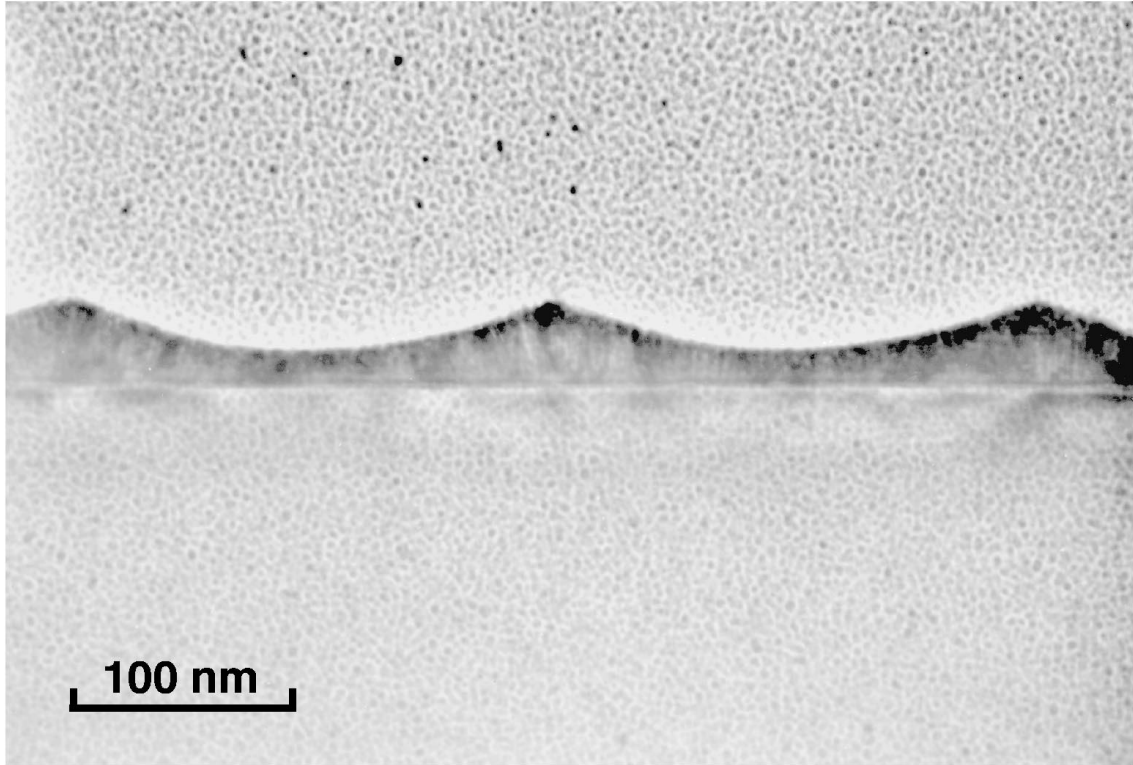


**Figure 8** Transmission electron microscope image of Cr lines formed by laser-focused atomic deposition. Shown is a cross section of the sample described in McClelland *et al.* (1993), obtained by coating the sample with quartz and sectioning it.

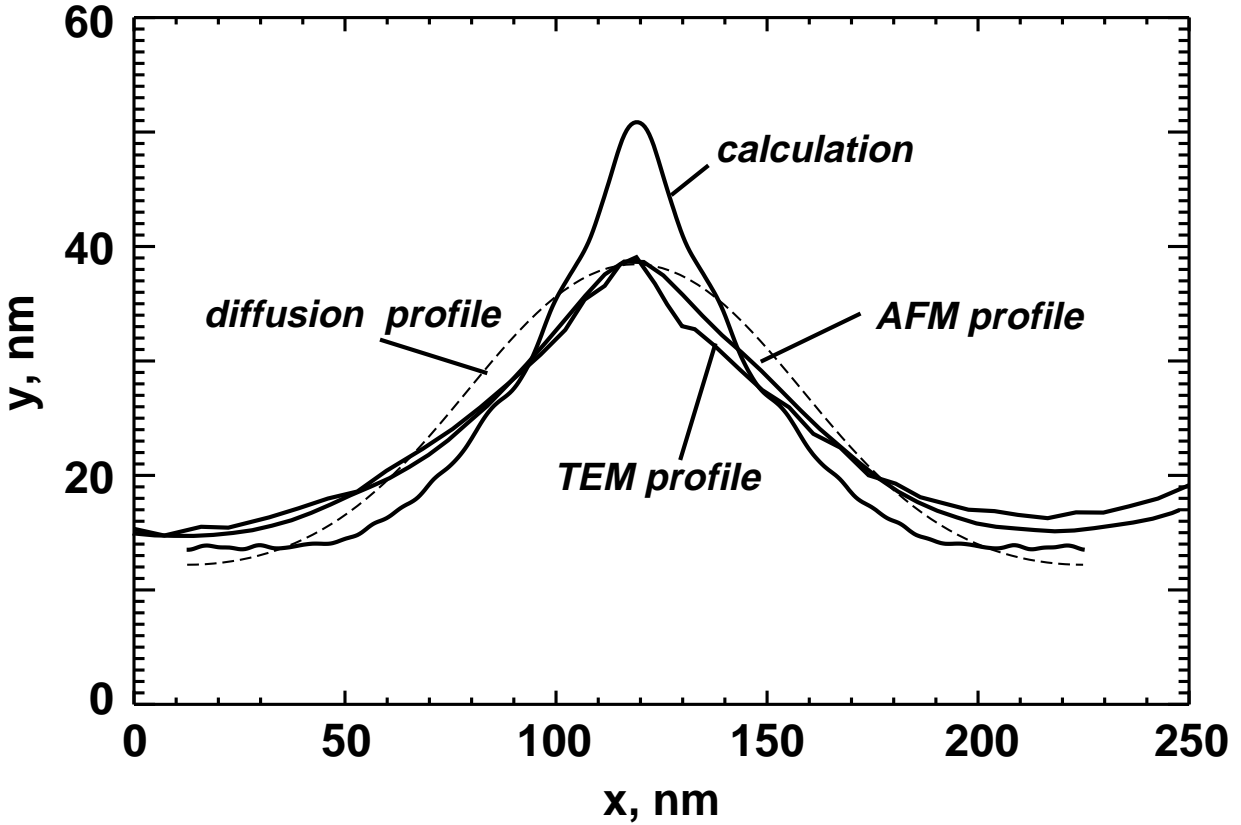


**Figure 9** Line profiles of a single line in laser-focused atomic deposition. The TEM profile is taken directly from Fig. 8. The AFM profile is taken from McClelland *et al.* (1993), scaled and shifted to correct for miscalibrations of the instrument and to account for the background. The calculation is the result of a ray tracing calculation (see text), and the diffusion profile is the result of a diffusion calculation applied to the ray-tracing result (see text).